International Journal of Solids and Structures 50 (2013) 2995–3007

Contents lists available at SciVerse ScienceDirect

International Journal of Solids and Structures

journal homepage: www.elsevier.com/locate/ijsolstr

A new approach to the analytical and numerical form-finding of tensegrity structures

K. Koohestani [a,*], S.D. Guest [b]

[a] Department of Structural Engineering, Faculty of Civil Engineering, University of Tabriz, Tabriz, Iran
[b] Department of Engineering, University of Cambridge, Trumpington Street, Cambridge CB2 1PZ, UK

ARTICLE INFO

Article history:
Received 19 January 2013
Received in revised form 14 May 2013
Available online 24 May 2013

Keywords:
Tensegrity structures
Form-finding
Force density
Equilibrium equations
Geometrical compatibility equations

ABSTRACT

We develop a new formulation for the form-finding of tensegrity structures in which the primary variables are the Cartesian components of element lengths. Both an analytical and a numerical implementation of the formulation are described; each require a description of the connectivity of the tensegrity, with the iterative numerical method also requiring a random starting vector of member force densities. The analytical and numerical form-finding of tensegrity structures is demonstrated through six examples, and the results obtained are compared and contrasted with those available in the literature to verify the accuracy and viability of the suggested methods.

1. Introduction

In 1947, a young artist named Kenneth Snelson invented and built a novel framework that he called floating compression. Later, Fuller (1962) called Snelson's structure a tensegrity, and since then, this nomenclature has been dominant in the scientific community. Tensegrity structures are pin-jointed, reticulated and self-equilibrated frameworks. A tensegrity is composed of a set of discontinuous compressive elements (called struts) floating within a net of continuous tensile elements (called cables). The rigidity of a tensegrity is the result of a self-stressed equilibrium between cables and struts. Tensegrities should be pre-stressed and usually need to have special geometries to provide self-equilibrated structural systems. The form-finding process determines a possible pre-stress distribution and geometry for a tensegrity. Early studies of the form-finding of tensegrities were performed by Fuller (1962) and Snelson (1965).

The form-finding of tensegrity structures has been widely studied through various analytical and numerical methods, where, typically, analytical methods are useful for studying tensegrities with small numbers of nodes and elements and tensegrities with high orders of symmetry. Previous analytical studies include: Connelly and Terrell (1995), who studied the analytical form-finding of rotationally symmetric tensegrities using the force density concept; Zhang et al. (2009a,b), who analytically studied the self-equilibrated states and stability of prismatic tensegrity structures; and Zhang et al. (2012, 2013) and Zhang and Ohsaki (2012), who developed unified analytical solutions for the self-equilibrium and super-stability of truncated regular polyhedral tensegrity structures. Static and dynamic characterisations of regular truncated icosahedral and dodecahedral tensegrities were also presented by Murakami and Nishimura (2001).

Numerical form-finding of tensegrity structures has been studied extensively using different methods, and some examples are given here, most of which ultimately employ the force density formulation first introduced by Schek (1974). Motro (1984) employed the dynamic relaxation method for the form-finding of tensegrity structures. Pellegrino (1986) proposed a nonlinear programming approach to the form-finding problem. The reduced coordinate method for the form-finding of tensegrity structures was introduced by Sultan et al. (1999) (see also Sultan, 1999). Masic et al. (2005) proposed an algebraic method, based on invariant tensegrity transformations, to solve the form-finding problem. Finite-element-based form-finding was developed by Pagitz and Mirats Tur (2009). Zhang et al. (2006) proposed an iterative method for the form-finding of tensegrity structures with geometrical and force constraints. Estrada et al. (2006) and Tran and Lee (2010a,b) proposed numerical methods for the form-finding of tensegrity structures which employ iterative eigenvalue and singular value decompositions of the force density and equilibrium matrices, with clear parallels with the numerical form-finding approach presented in Section 5. The adaptive force density method introduced by Zhang and Ohsaki (2006) also utilised spectral decomposition of force density matrix as a core part of the form-finding process. As a stochastic approach, Li et al. (2010) used

* Corresponding author. Tel.: +98 411 3392391; fax: +98 411 3356024.
E-mail addresses: kk484@eng.cam.ac.uk, ka_koohestani@tabrizu.ac.ir (K. Koohestani).

0020-7683/$ - see front matter © 2013 Elsevier Ltd. All rights reserved.
http://dx.doi.org/10.1016/j.ijsolstr.2013.05.014

Monte Carlo methods to find equilibrium configurations of large-scale regular and irregular tensegrity structures. Rieffel et al. (2009) introduced a special evolutionary form-finding method, Koohestani (2012), Paul et al. (2005) and Xu and Luo (2010) used genetic algorithms and Chen et al. (2012) used ant colony systems for the form-finding of tensegrities. Mathematical programming has also been used in the form-finding and optimisation of tensegrity structures under different constraints, including discontinuity of struts, compliance, stress and self-weight loads. In this category, we may refer to the mixed integer programming approach of Ehara and Kanno (2010) and Kanno (2011, 2012). Recent reviews of the form-finding and analysis of tensegrities may be found in Hernàndez Juan and Mirats Tur (2008), Mirats Tur and Hernàndez Juan (2009), Sultan (2009) and Tibert and Pellegrino (2003).

In this paper, we introduce a combined form of the equilibrium and geometrical compatibility equations for tensegrity structures. By considering the connectivity of a tensegrity as a directed graph, geometrical compatibility equations are effectively generated by its cycle basis. The interrelation between the current formulation and the force density formulation is established, and analytical and numerical form-finding methods are proposed. Six examples are studied using our analytical and numerical methods, and the results obtained are compared with those documented in the literature.

2. Equilibrium equations

In this section we present the equilibrium equations for a 3-dimensional tensegrity structure (the restriction to 2-dimensions is straightforward). We will first describe a conventional formulation where the geometry is fixed and the primary variables are force density in the members, briefly mention the force density formulation where the force density is fixed and the positions of nodes are the primary variables, and then we will present a novel formulation where the primary variables are Cartesian components of element lengths.

Consider a typical node shown in Fig. 1. The equilibrium (for instance in the x-direction) can be written as

$$f_i^x = \sum_{r\in I} f_{ir}^x = \sum_{r\in I} \frac{f_{ir}(x_i - x_r)}{L_{ir}} = p_i^x \tag{1}$$

Here, I is a set that contains labels of all nodes adjacent (connected) to node i, f_{ir} and L_{ir} are the internal force and length of an element with i and r as its start and end nodes, respectively. Also, p_i^x is

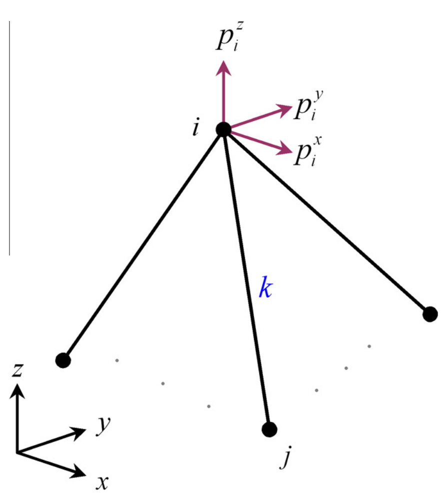

Fig. 1. Typical nodes (i,j) and element (k) of a tensegrity with external forces at node i.

the external force at node i and in the x-direction. If we label each element ij with a single number k (between 1 and m) then we can write f_{ir}^x based on element's force density as follows:

$$f_{ij}^x = \frac{f_{ij}(x_i - x_j)}{L_{ij}} = \frac{f_k(x_i - x_j)}{L_k} = q_k(x_i - x_j) \tag{2}$$

where $q_k = f_{ij}/L_{ij} = f_k/L_k$ is the force density of element k. A similar equation can simply be written for the other end (node j) as given in Eq. (3).

$$f_{ji}^x = q_k(x_j - x_i) \tag{3}$$

A compact matrix form of Eqs. (2) and (3) is

$$\begin{bmatrix} f_{ij}^x \\ f_{ji}^x \end{bmatrix} = \begin{bmatrix} -1 \\ 1 \end{bmatrix} q_k d_k^x \tag{4}$$

where $d_k^x = x_j - x_i$. In fact, by considering element k as a vector directed from node i to j with length L_k, d_k^x is the Cartesian component (projection) of the length of this vector in the x-direction. It is straightforward to write similar equations for all other elements and in the y- and z-directions.

If we wish to consider force densities as primary variables, we can use the above equations to write the equilibrium equations for every node and every direction (for a 3-dimensional tensegrity with n nodes and m elements) as the matrix equation,

$$\mathbf{A}\mathbf{q} = \begin{bmatrix} \mathbf{p}_x \\ \mathbf{p}_y \\ \mathbf{p}_z \end{bmatrix} \tag{5}$$

where $\mathbf{q} = [q_1, q_2, \ldots, q_m]^t$, $\mathbf{p}_x = [p_1^x, p_2^x, \ldots, p_m^x]^t$, $\mathbf{p}_y = [p_1^y, p_2^y, \ldots, p_m^y]^t$, $\mathbf{p}_z = [p_1^z, p_2^z, \ldots, p_m^z]^t$ and $\mathbf{A} \in \mathbf{R}^{3n\times m}$ is a rectangular matrix as follows:

$$\mathbf{A} = \begin{bmatrix} \mathbf{B}\ diag(\mathbf{d}_x) \\ \mathbf{B}\ diag(\mathbf{d}_y) \\ \mathbf{B}\ diag(\mathbf{d}_z) \end{bmatrix} \tag{6}$$

In Eq. (6), $\mathbf{d}_x = [d_1^x, d_2^x, \ldots, d_m^x]^t$, $\mathbf{d}_y = [d_1^y, d_2^y, \ldots, d_m^y]^t$, $\mathbf{d}_z = [d_1^z, d_2^z, \ldots, d_m^z]^t$ and $\mathbf{B} = [b_{ij}]_{n\times m}$ is defined as

$$b_{ij} = \begin{cases} -1 & \text{if} \quad i \text{ is the start node of element } j \\ 1 & \text{if} \quad i \text{ is the end node of element } j \\ 0 & \text{otherwise} \end{cases} \tag{7}$$

From a graph-theoretical point of view, $\mathbf{B}$ is the node-element incidence matrix for a directed graph where each element is directed from node i to j ($i < j$). In addition, the rank of $\mathbf{B}$ is $n - 1$ (Kaveh, 2004), which means that its rows are linearly dependent.

Matrix $\mathbf{A}$ is defined by Pellegrino and Calladine (1986) as the equilibrium matrix, although that term is also commonly used for the equivalent matrix in which each column is divided by the length of the corresponding member (see e.g., Pellegrino, 1993).

If we wish to consider the nodal positions as primary variables, we can use the force density formulation (Schek, 1974). In general, the equilibrium equations for a structure can be written as

$$\mathbf{F}_{int} = \mathbf{P}_{ext} \tag{8}$$

where $\mathbf{F}_{int}$ and $\mathbf{P}_{ext}$ are internal and external nodal forces matrices in the global coordinates system. For a 3-dimensional tensegrity with n nodes and m elements, we define

$$\mathbf{F}_{int} = [\mathbf{f}_x, \mathbf{f}_y, \mathbf{f}_z] = \begin{bmatrix} f_1^x & f_1^y & f_1^z \\ f_2^x & f_2^y & f_2^z \\ \vdots & \vdots & \vdots \\ f_n^x & f_n^y & f_n^z \end{bmatrix} \tag{9}$$

$$\mathbf{P}_{ext} = [\mathbf{p}_x, \mathbf{p}_y, \mathbf{p}_z] = \begin{bmatrix} p_1^x & p_1^y & p_1^z \\ p_2^x & p_2^y & p_2^z \\ \vdots & \vdots & \vdots \\ p_n^x & p_n^y & p_n^z \end{bmatrix} \tag{10}$$

By substituting Eq. (1), and similar equations for y- and z-directions, into Eq. (9), we can write the equilibrium equations as

$$\mathbf{SN} = \mathbf{P}_{ext} \tag{11}$$

where $\mathbf{N} = [\mathbf{x}, \mathbf{y}, \mathbf{z}]$ is the matrix of nodal coordinates ($\mathbf{x} = [x_1, x_2, \ldots, x_n]^t$, $\mathbf{y} = [y_1, y_2, \ldots, y_n]^t$ and $\mathbf{z} = [z_1, z_2, \ldots, z_n]^t$), and $\mathbf{S}$ is the force density matrix, also sometimes called the stress matrix (see e.g., Connelly and Terrell, 1995 and Guest, 2006).

In this paper, however, we choose not to use nodal positions as primary variables, but Cartesian components of element lengths. By considering Eqs. (1) and (4) and combining them for all elements and in all directions, equilibrium equations are obtained for entire structure as

$$\mathbf{BQD} = \mathbf{P}_{ext} \tag{12}$$

where $\mathbf{Q} = diag(\mathbf{q})$ is the diagonal matrix of force densities, and $\mathbf{D} \in \mathbf{R}^{m \times 3}$ is the matrix of Cartesian components of element lengths,

$$\mathbf{D} = [\mathbf{d}_x, \mathbf{d}_y, \mathbf{d}_z] \tag{13}$$

Eq. (12) described the equilibrium equations for a 3-dimensional tensegrity structure to which external forces have been applied. However, we are interested here in the case the structure has a state of self-stress with no external loads applied, i.e.

$$\mathbf{BQD} = \mathbf{BQ}[\mathbf{d}_x, \mathbf{d}_y, \mathbf{d}_z] = [\mathbf{0}, \mathbf{0}, \mathbf{0}] \tag{14}$$

Similarly, the right hand side of Eq. (5) will also be zero, i.e. $\mathbf{p}_x = \mathbf{p}_y = \mathbf{p}_z = \mathbf{0}$ and so $\mathbf{Aq} = \mathbf{0}$.

If the structure is 3-dimensional, $\mathbf{d}_x, \mathbf{d}_y$ and $\mathbf{d}_z$ must be three independent vectors (see e.g., Connelly, 1982), and hence the null-space of $\mathbf{BQ}$ must be at least 3-dimensional. However, this is not a sufficient condition, as we do not have a free choice for $\mathbf{d}_x, \mathbf{d}_y$ and $\mathbf{d}_z$ — these vectors must also be geometrically feasible. The next section will consider the geometrical compatibility.

3. Geometrical compatibility equations

This section will consider the geometrical compatibility relationships for tensegrity structures. Consider as an example a simple 2-dimensional pin-jointed structure (see Fig. 2(a)), with all its nodes and elements labelled. We consider each element as a directed edge from a connectivity point of view, and as a vector from a geometrical point of view. The connectivity model for the structure is a simple directed graph in which each edge is directed from node i to j ($i < j$). In a consistent geometry, the following equations must be valid for the structure in Fig. 2 irrespective of the numerical values of nodal coordinates.

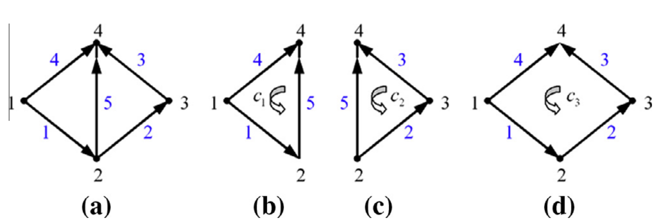

Fig. 2. (a) Graph model of a simple pin-jointed structure; (b) first cycle (elements 1 and 5 are positively directed and element 4 is negatively directed in this cycle); (c) second cycle (elements 2 and 3 are positively directed and element 5 is negatively directed in this cycle); (d) third cycle (elements 1, 2 and 3 are positively directed and element 4 is negatively directed in this cycle).

$$\mathbf{v}_1 + \mathbf{v}_5 - \mathbf{v}_4 = \mathbf{0}$$

$$\mathbf{v}_2 + \mathbf{v}_3 - \mathbf{v}_5 = \mathbf{0}$$

$$\mathbf{v}_1 + \mathbf{v}_2 + \mathbf{v}_3 - \mathbf{v}_4 = \mathbf{0}$$

Here, $\mathbf{v}_k$ is a vector associated with element k (with i and j as start and end nodes), and it is defined as $\mathbf{v}_k = [d_k^x, d_k^y, d_k^z]^t = [x_j - x_i, y_j - y_i, z_j - z_i]^t$. These equations are linearly dependent and each one can be obtained by a linear combination of the others. We select the first two equations and write these equations as

$$\begin{bmatrix} 1 & 0 & 0 & -1 & 1 \\ 0 & 1 & 1 & 0 & -1 \end{bmatrix} \begin{bmatrix} d_1^x & d_1^y & d_1^z \\ d_2^x & d_2^y & d_2^z \\ d_3^x & d_3^y & d_3^z \\ d_4^x & d_4^y & d_4^z \\ d_5^x & d_5^z & d_5^z \end{bmatrix} = \begin{bmatrix} 0 & 0 & 0 \\ 0 & 0 & 0 \end{bmatrix} \tag{15}$$

The coefficient matrix in Eq. (15) has a special pattern from the labelling of its elements. The matrix is called a cycle-member incidence (cycle basis) matrix because each row corresponds to a cycle in the underlying graph. The first and second rows correspond to cycles $c_1 = \{1,4,5\}$ and $c_2 = \{2,3,5\}$, respectively (see Fig. 2(b) and (c)).

For a simple directed graph, the cycle-member incidence matrix is usually denoted by $\mathbf{C} = [c_{ij}]_{\beta \times m}$ and is defined as follows:

$$c_{ij} = \begin{cases} -1 & \text{if} \quad j \text{ is in } c_i \text{ and negatively directed} \\ 1 & \text{if} \quad j \text{ is in } c_i \text{ and positively directed} \\ 0 & \text{otherwise} \end{cases} \tag{16}$$

For a connected graph with m members and n nodes, $\beta = m - n + 1$ is the dimension of the cycle space (the maximum number of independent cycles) and is often referred to as the graph *cyclomatic number*, *nullity* or *first Betti number* (see, e.g., Berge, 2001). The reader may refer to Micheletti (2008) for a recent application of the cycle basis for generating reciprocal diagrams for self-stressed frameworks. The cycle-member incidence matrix is related to the node-member incidence matrix by the orthogonality relationship,

$$\mathbf{BC}^t = \mathbf{0}_{n \times \beta}, \quad \mathbf{CB}^t = \mathbf{0}_{\beta \times n} \tag{17}$$

We use this feature of a cycle-member incidence matrix to establish an interrelation between the current formulation and the force density formulation. Considering the above definitions, it is possible to define the geometrical compatibility equations of a tensegrity structure in terms of Cartesian components of element lengths as given in Eq. (18)

$$\mathbf{C}[\mathbf{d}_x, \mathbf{d}_y, \mathbf{d}_z] = \mathbf{CD} = [\mathbf{0}, \mathbf{0}, \mathbf{0}] \tag{18}$$

3.1. Automated generation of geometrical compatibility equations

According to Eq. (18), we only need to find the cycle basis of a graph (the graph of a tensegrity) to write the geometrical compatibility equations. The cycle basis of a graph is a very well-covered subject in the field of combinatorial mathematics, and various methods to form this basis have been proposed. All types of cycle bases are valid for use within our formulation. However, the minimal cycle basis is advantageous, as it enables us to reduce the computational effort, and to find simpler relationships between force densities during analytical form-finding. In fact, a minimal cycle basis leads to a cycle-member incidence matrix with a very sparse form. Analytical form-finding presented later requires a sparse cycle basis matrix to provide a significant reduction in the total number of symbolic operations and fill-ins, which leads to simpler entries in the final factorised matrix. Note that for simple graphs it is straightforward to generate a minimal cycle basis simply by examining all the cycles, however, the reader may refer to De Pina (1995), Horton (1987), Kavitha et al. (2008) and Mehlhorn and Michail (2009), among others, for some efficient algorithms for the generation of the minimal cycle basis.

The geometrical compatibility equations can also be generated simply and numerically. To do so, we need to obtain a null-space basis of $\mathbf{B}$ (the columns of $\mathbf{C}^t$ form a basis for the null space of $\mathbf{B}$). Both a triangular basis, usually formed by the Gauss–Jordan elimination method, and an orthonormal basis, usually formed by singular value decomposition (SVD), are acceptable. Note that an orthonormal basis is completely dense (all its entries are nonzero) while a triangular basis can be moderately sparse. The sparsity of a triangular basis can be improved by performing a special type of Gauss elimination method; see Soyer and Topçu (2001) for more detail.

4. Combined form of equations and self-stressed states

In the preceding sections, we have presented the equilibrium equations (Eq. (14)) and geometrical compatibility equations (Eq. (18)). The primary variables for both sets of equations are the same; hence, the two sets of equations can be combined to obtain a new set of equations, as follows:

$$\mathbf{HD} = \begin{bmatrix} \mathbf{C} \\ \mathbf{BQ} \end{bmatrix} \mathbf{D} = [\mathbf{0}, \mathbf{0}, \mathbf{0}] \tag{19}$$

Here, $\mathbf{H} \in \mathbf{R}^{m+1 \times m}$ (total number of rows is $\beta + n = m + 1$). It is clear that a non-trivial solution of Eq. (19) satisfies both equations of equilibrium and of geometrical compatibility simultaneously. To form a 3-dimensional tensegrity, the rank of $\mathbf{H}$ must be at most $m - 3$, because of the necessity of finding three independent null vectors.

It is interesting to compare the formulation given in Eq. (19) with the conventional force density formulation (Eq. (11)). Clearly, Eq. (19) can be transformed to Eq. (11) by noting that

$$\mathbf{B}^t\mathbf{N} = \mathbf{D} \tag{20}$$

and $\mathbf{CB}^t = \mathbf{0}$, showing that $\mathbf{S} = \mathbf{BQB}^t$. Thus, essentially our formulation is an expanded form of the force density formulation. In three dimensions, the force density method works with $3n$ nodal coordinates, while our formulation works with $3m$ components of member lengths (where, typically, $m > n$). We lose the square and symmetric nature of the matrix, but gain from the potential for the sparse nature of $\mathbf{H}$, particularly for analytical form-findings.

The difference between our formulation and the force density formulation is very similar to the difference between the force and displacement methods for structural analysis. In the displacement method, the equilibrium equations are written based on the stiffness matrix and the nodal displacements, which automatically satisfy compatibility conditions. In the standard force method, both the equilibrium and the compatibility conditions are written individually, based on elements' independent forces, and should be satisfied simultaneously. In fact, our formulation is analogous to the integrated force method (IFM) that was developed by Patnaik (1986). The reader can recognise the difference between the compatibility of displacements (used in the standard and integrated force methods) and the geometrical compatibility conditions described here.

5. Form-finding

The requirements of our formulation can be considered as two-fold: we require the force densities to form a state of self-stress, i.e. satisfy $\mathbf{Aq} = \mathbf{0}$, and we require there to be, for a 3-dimensional tensegrity, three independent solutions to $\mathbf{HD} = \mathbf{0}$ (or two independent solutions in 2-dimensions). In fact, as the matrix $\mathbf{H}$ combines equilibrium and compatibility conditions, the latter requirement completely implies the former; however, in practice it can be helpful to separately and explicitly consider the equilibrium condition.

5.1. Analytical method

In order to give an analytical formulation, in this paper we use Gaussian elimination with a pivoting strategy to analytically convert $\mathbf{H}$ to an upper triangular matrix. By ensuring that the final rows of this upper triangular matrix are all zero, the relationships required between the force densities in different members for them to form a state of self-stress can be obtained. However, to carry out these calculations, a computing platform with symbolic computation capabilities, such as *Maple* or *Matlab*, is advantageous. In order to reduce the total number of symbolic operations and to keep the final matrix as simple as possible, two points should be taken into consideration. First, the pivot entries should be kept as simple as possible by performing suitable row permutations. Second, in choosing between rows with simple and suitable pivot entries, those with the least nonzero entries (sparser rows) are more appropriate for use as a pivot row. Note that performing simultaneous row and column permutations can further improve the above process, however for the examples presented in Section 6, we only performed row permutations. For the analytical formulation we do not separately consider the equilibrium matrix $\mathbf{A}$.

5.2. Numerical method

We also consider a numerical and iterative form-finding method based on our formulation. The method requires the following data for initialisation:

(a) Connectivity data. The matrices $\mathbf{B}$ and $\mathbf{C}$ can be generated using connectivity data and the definitions and procedures described so far.
(b) A random vector of force densities, denoted by $\mathbf{q}^0$. Note that a suitable sign should be assigned to each entry according to the type of the corresponding element (positive for tensile members and negative for compressive elements).

After the above initialisation steps, we calculate an orthonormal basis for the null space of $\mathbf{C}$, denoted by $\mathbf{N}_c \in \mathbf{R}^{m \times n-1}$, as a general solution for compatibility equations. As a result, every geometrically compatible solution, including a solution (if one exists) that satisfies equilibrium can be formed by linear combination of columns of $\mathbf{N}_c$. Therefore, $\mathbf{D}$ is considered as

$$\mathbf{D} = \mathbf{N}_c\mathbf{T} \tag{21}$$

where $\mathbf{T} \in \mathbf{R}^{n-1 \times 3}$ is a rectangular matrix that contains coefficients of the linear combination of columns. As a particular solution, $\mathbf{D}$ should also satisfy equilibrium equations (Eq. (14)), and we obtain

$$\mathbf{GT} = [\mathbf{0}, \mathbf{0}, \mathbf{0}] \tag{22}$$

where $\mathbf{G} \in \mathbf{R}^{n \times n-1}$ and $\mathbf{G} = \mathbf{BQN}_c$.

For a set of force densities that form a state of self-stress, $\mathbf{T}$ can simply be calculated as null-space basis of $\mathbf{G}$. However, if we only have an approximate set of force densities, denoted by $\mathbf{Q}^i$ in iteration i, we can calculate an approximation of $\mathbf{T}^i$ by minimising the 2-norm of the residual force matrix as follows:

$$\underset{\mathbf{T}}{Minimise} \left\| \mathbf{G}^i \mathbf{T}^i \right\|_2 \tag{23}$$

In order to determine a $\mathbf{T}^i$ that satisfies Eq. (23), we use the SVD of $\mathbf{G}^i = \mathbf{B}\mathbf{Q}^i\mathbf{N}_c$

$$\mathbf{G}^i = \left(\mathbf{U}_G\mathbf{V}_G\mathbf{W}_G^t\right)^i \tag{24}$$

Based on this decomposition, the best approximation of $\mathbf{T}^i$ is obtained using the vectors of $(\mathbf{W}_G)^i$ associated with the three smallest singular values of $\mathbf{G}^i$ (the last three diagonal entries of $(\mathbf{V}_G)^i$), leading to better approximations of the element projection lengths, $\mathbf{D}^{i+1}$. The new values of $\mathbf{d}_x^{i+1}, \mathbf{d}_y^{i+1}$ and $\mathbf{d}_z^{i+1}$ are then employed in Eq. (6) to calculate the coefficient matrix of equilibrium equations ($\mathbf{A}^{i+1}$). In a self-stress state, $\mathbf{A}$ has at least one zero singular value, and by using a similar approach to the one described above, we can find a new approximation of force densities that form a state of self-stress $\mathbf{q}^{i+1}$. We need to find a new set of force densities in a way that satisfies the minimisation problem

$$\underset{\mathbf{q}}{Minimise} \left\| \mathbf{A}^{i+1}\mathbf{q}^{i+1} \right\|_2 \tag{25}$$

$$Subject\ to: \mathrm{sgn}(\mathbf{q}^{i+1}) = \mathrm{sgn}(\mathbf{q}^0)$$

where 'sgn' denotes sign function. In order to solve the above minimisation problem, the SVD of $\mathbf{A}^{i+1}$ is calculated as $\mathbf{A}^{i+1} = (\mathbf{U}_A\mathbf{V}_A\mathbf{W}_A^t)^{i+1}$, and the last column of $(\mathbf{W}_A)^{i+1}$ corresponding to the smallest singular value is selected as the new vector of force densities. Element types are imposed *a priori*, meaning that the sign of the force density vector obtained from the SVD of $\mathbf{A}^{i+1}$ should be the same as $\mathbf{q}^0$ in all iterations (see the constraint defined in Eq. (25)). Although note that the overall sign is not important at this stage, and is indeed arbitrary in the SVD. However, to ensure that the sign of an iterative set of force densities conforms to $\mathbf{q}^0$, we adopt Estrada et al.'s (2006) approach, which employs linear combinations of the other columns of $\mathbf{W}_A$ within a least square approximation to find a vector whose sign matches with the initial set of force densities.

The above steps can be employed iteratively to minimise the residual forces as much as is required. Iterations cease when the stopping criterion, as defined in Eq. (26), is satisfied.

$$t = \max(t_1, t_2) \leqslant \varepsilon \tag{26}$$

Here, t_1 is the maximum value of the three smallest singular values of $\mathbf{G}^i$ and t_2 is the smallest singular value of $\mathbf{A}^{i+1}$. The user sets ε as a very small number according to the desired level of accuracy.

After convergence, the nodal coordinates of tensegrity should be calculated using Eq. (20). Different methods can be used to solve Eq. (20); we offer a solution based on the Moore–Penrose pseudo-inverse (see Golub and Van Loan, 1996 for more detail) of $\mathbf{B}^t$ as follows:

$$\mathbf{N} = [\mathbf{x}, \mathbf{y}, \mathbf{z}] = \left(\mathbf{B}^t\right)^+\mathbf{D} \tag{27}$$

Here, the superscript + on $\mathbf{B}^t$ refers to the Moore–Penrose pseudo-inverse operator. This method promises to find a solution of Eq. (20) in such a way that the norms of vectors $\mathbf{x}, \mathbf{y}$ and $\mathbf{z}$ are smaller than the norms of any other possible solution.

Note that, as the SVD is employed throughout of the iterations, we always obtain an orthogonal matrix of Cartesian components of element lengths as follows:

$$\mathbf{D}^t\mathbf{D} = \begin{bmatrix} \mathbf{d}_x^t\mathbf{d}_x & \mathbf{d}_x^t\mathbf{d}_y & \mathbf{d}_x^t\mathbf{d}_z \\ \mathbf{d}_y^t\mathbf{d}_x & \mathbf{d}_y^t\mathbf{d}_y & \mathbf{d}_y^t\mathbf{d}_z \\ \mathbf{d}_z^t\mathbf{d}_x & \mathbf{d}_z^t\mathbf{d}_y & \mathbf{d}_z^t\mathbf{d}_z \end{bmatrix} = \begin{bmatrix} 1 & 0 & 0 \\ 0 & 1 & 0 \\ 0 & 0 & 1 \end{bmatrix} \tag{28}$$

Considering the trace of the above matrix, this orthogonality leads to a special constraint on the final geometry of a 3-dimensional tensegrity, concerning the length of elements, as follows:

$$\sum_{i=1}^{m} L_i^2 = 3 \tag{29}$$

The above features lead to a tensegrity structure geometry without any dilation, shear or translation. In the following, the process of our numerical form-finding method is presented in a step-by-step algorithmic form.

Algorithm

Step 1. Define connectivity data and a random set of force densities ($\mathbf{q}^0$).
Step 2. Form $\mathbf{B}$ and $\mathbf{C}$ and calculate $\mathbf{N}_c$ (also $\mathbf{E}$, see 5.3). Set $i = 0$.
Step 3. Calculate the SVD of $\mathbf{G}^i = \mathbf{B}\mathbf{Q}^i\mathbf{N}_c$ and select $\mathbf{T}^i$.
Step 4. Calculate $\mathbf{D}^{i+1} = \mathbf{N}_c\mathbf{T}^i$.
Step 5. Calculate the SVD of $\mathbf{A}^{i+1}$ (or $\mathbf{A}_E^{i+1}$) and select $\mathbf{q}^{i+1}$ (see 5.3 for more details).
Step 6. If $t \leqslant \varepsilon$ stop; else $i = i + 1$ and continue from step 3.

5.3. Symmetry and grouping of elements

It may be required that the found form for a tensegrity has certain symmetry. According to the required symmetry, elements can be grouped, and one force density associated with all elements of each group. As a result, grouping reduces the total number of variables in the analytical form-finding—note that grouping can be considered independent of the symmetry of a tensegrity. The reader may refer to Murakami and Nishimura (2001), Sultan et al. (2001), Tibert and Pellegrino (2003), Zhang et al. (2009a,b) and Zhang et al. (2010), for some examples of exploiting symmetry and grouping in the analytical form-finding and characterisation of tensegrity structures. In numerical form-finding, grouping can also be considered for symmetric tensegrities. A problem in numerical form-finding methods relating to grouping arises from the different approximations used to iteratively calculate the vector of force densities. In our method, step 5 is sensitive to grouping. An approximated vector of force densities (the last column of $(\mathbf{W}_A)^{i+1}$) does not necessarily follow the initial grouping scheme. An efficient approach is proposed here to address this problem. The method is completely general and can be used as part of any numerical form-finding method that uses similar approximation steps.

Let all elements of a tensegrity be packed into k groups, denoted by $g_1, g_2, \ldots, g_k$, where each group is a set that contains labels of all elements with the same force density. For a typical group g_j, $|g_j| - 1$ independent equations ($|\cdot|$ means cardinality of a set) can be associated based on equality relationships between the force densities of elements. For example, let l and p be in a group. The equality $q_l = q_p$ leads to the equation $(\mathbf{e}_l^t - \mathbf{e}_p^t)\mathbf{q} = 0$ where $\mathbf{e}_l$ and $\mathbf{e}_p$ are m-dimensional base vectors. Considering all groups, $\left(\sum_{j=1}^{k}|g_j|\right) - k$ independent equations can be generated in matrix form as follows:

$$\mathbf{E}\mathbf{q} = \mathbf{0} \tag{30}$$

Eq. (30) can be combined by the equilibrium equations, $\mathbf{A}\mathbf{q} = \mathbf{0}$, leading to an augmented form of the equilibrium equations as given in Eq. (31).

$$\mathbf{A}_E\mathbf{q} = \begin{bmatrix} \mathbf{A} \\ \mathbf{E} \end{bmatrix}\mathbf{q} = \mathbf{0} \tag{31}$$

For symmetric tensegrities including an initial grouping, the SVD of $\mathbf{A}_E$ should be calculated instead of that of $\mathbf{A}$. In the early stages of the form-finding process, the approximate solution of

Eq. (31) again leads to $\mathbf{Eq} \approx \mathbf{0}$, but with less diversity. We require a final step to completely remove any inconsistency in the force density vector. To do so, $\mathbf{q}^{i+1}$ is created such that the mean force density of all elements in each group is selected as the force density associated with the elements of that group. After the final adjustment, it is clear that the vector of force densities follows the initial grouping scheme.

5.4. Convergence

In numerical analysis, an iterative method is called globally convergent if the successive approximations generated by the method converge to a feasible solution (or the same solution for the problems with a unique solution) starting from arbitrary initial approximations. However, in practice, most iterative methods are locally convergent and should be provided with reasonably good initial approximations to converge to a solution. Our study shows that the numerical form-finding method proposed in this paper has been found to converge to a solution for all sets of random force densities tried, although some solutions may not be feasible. From this numerical experiment point of view, our method is locally convergent. The unfeasible solutions typically arise, for instance, if an initial random set of force densities, $\mathbf{q}^0$, leads to a geometry including one or more elements with zero (or very small) lengths or force densities. We can identify this condition by using $L_{\max}/L_{\min}$ as an indicator, where $L_{\max}$ and $L_{\min}$ are the maximum and minimum lengths of elements, respectively. Note that the length of each element can be calculated in step 4 of the algorithm after the calculation of $\mathbf{D}^{i+1}$ by using $L_j = \sqrt{dx_j^2 + dy_j^2 + dz_j^2}, j = 1, 2, \ldots, m$. A very large value for the above fraction (e.g., 20 or more) may be a good indicator of an improper $\mathbf{q}^0$. The same restriction may also be applied to $\max|\mathbf{q}|/\min|\mathbf{q}|$. Overall, our study reveals that, although the convergence (and its rate) of the proposed method is generally dependent on two different variables (i.e. the topology of tensegrity and the initial random set of force densities), it still converges satisfactorily in practice for a wide variety of random initialisations.

6. Examples

In this section, five examples of well-known tensegrities and an example of a new tensegrity are provided. Their self-stress states and found forms are studied through our analytical and numerical approaches. The first two examples use the analytical approach and include details about cycle bases and their connections to our formulation. The third example is studied both numerically and analytically. For the sake of brevity, details about cycle bases are not provided for the last four examples. In all examples, we assume that the symmetry properties of a tensegrity (in a geometrical manner) cannot be exploited or unknown. However, element grouping is available throughout. In all numerical procedures, the convergence criterion ε is set to 1×10^{-15}.

6.1. Example 1

In this example, the self-equilibrium state of a 2-dimensional tensegrity is studied using the analytical method proposed (restriction of the formulations to 2-dimensional tensegrities is straightforward). Fig. 3 shows a graph model of the tensegrity with its elements labelled. This graph has $n = 6$ nodes and $m = 9$ elements. We consider four groups of elements, two sets of cables $g_1 = \{1, 3, 4, 6\}$, $g_2 = \{2, 5\}$ and two sets of struts $g_3 = \{7, 8\}$ and $g_4 = \{9\}$. Furthermore, q_1, q_2, q_3 and q_4 are associated with these groups as their respective force densities. The cyclomatic number of this graph is 4. Therefore, four independent cycles,

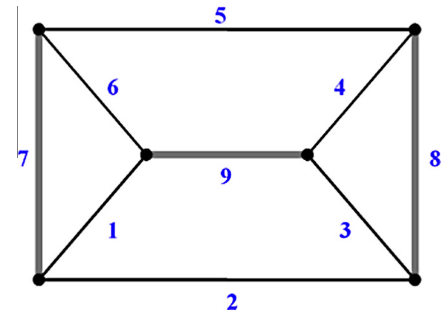

Fig. 3. Graph model of a 2-dimensional tensegrity.

$c_1 = \{1^+, 6^-, 7^+\}$, $c_2 = \{1^+, 2^+, 3^+, 9^-\}$, $c_3 = \{3^+, 4^+, 8^-\}$ and $c_4 = \{4^+, 5^+, 6^-, 9^+\}$ form its cycle basis. The set of cycles is minimal as it is not possible to find another set of cycles with a smaller number of elements. In addition, the sign attached to each number refers to the right sign of the corresponding nonzero entry in the cycle-member incidence matrix $\mathbf{C}$. We generate the combined form of the equilibrium and geometrical compatibility equations ($\mathbf{H}$) and apply the analytic procedure described in Section 5.1 to create an upper triangular matrix, denoted by $\mathbf{H}'$, as follows:

$$\mathbf{H}' = \begin{bmatrix} 1 & 0 & 0 & 0 & 0 & -1 & 1 & 0 & 0 \\ 0 & 1 & 1 & 0 & 0 & 1 & -1 & 0 & -1 \\ 0 & 0 & 1 & 1 & 0 & 0 & 0 & -1 & 0 \\ 0 & 0 & 0 & 1 & 1 & -1 & 0 & 0 & 1 \\ 0 & 0 & 0 & 0 & q_2 & q_1 & q_3 & 0 & 0 \\ 0 & 0 & 0 & 0 & 0 & -2q_1 & q_1 & 0 & -q_4 \\ 0 & 0 & 0 & 0 & 0 & 0 & \alpha & q_2 & 0 \\ 0 & 0 & 0 & 0 & 0 & 0 & 0 & \beta & \gamma \\ 0 & 0 & 0 & 0 & 0 & 0 & 0 & 0 & -2\gamma \\ 0 & 0 & 0 & 0 & 0 & 0 & 0 & 0 & 0 \end{bmatrix}$$

Here, $\alpha = -(q_1 + q_2 + 2q_3)$, $\beta = \frac{(q_1+2q_3)(q_1+2q_2+2q_3)}{-2\alpha}$ and $\gamma = -\frac{2q_1q_2+q_1q_4+2q_2q_4}{2q_2}$.

Matrix $\mathbf{H}'$ has 9 columns and 10 rows, and hence for any set of parameters, all entries of the last row of $\mathbf{H}'$ must be zero. To give two independent solutions for $\mathbf{d}_x$ and $\mathbf{d}_y$ (as we are considering a 2-dimensional tensegrity) the rank of $\mathbf{H}$ should be $9 - 2 = 7$. This rank can be achieved if both β and γ are zero. From $\gamma = 0$ we obtain $q_4 = -2q_1q_2/(q_1 + 2q_2)$, while for $\beta = 0$ there are two possible cases: $q_3 = -q_1/2$ or $q_3 = -(q_1 + 2q_2)/2$. The first case corresponds to a super-stable configuration (see Connelly and Terrell, 1995 and Zhang and Ohsaki, 2007 for more detail about super-stability conditions) while the second one does not. In fact the second case is neither super-stable nor stable because its linear elastic stiffness matrix is not positive definite (excluding rigid body motions). Note that, tensegrities without super stability may still be stable — for these cases, however, the stability can be investigated based on prestress/stiffness ratio of elements and spectral characteristics of the tangent stiffness matrix (sum of the linear elastic stiffness and geometrical stiffness matrices). The reader may refer to Ohsaki and Zhang (2006) for the necessary and sufficient conditions for the stability of pin-jointed structures including tensegrities.

The second equation for q_3 sets four diagonal entries of the force density matrix equal to $-q_2$, a negative value, and annihilates the positive semi-definiteness of the force density matrix. To verify the formulation and the results, eigenvalues of the force density matrix are calculated symbolically using the above relationships between the force densities. For the first case, three zero-valued eigenvalues are obtained. The other three eigenvalues are $3q_1$, $2q_2$ and $(3q_1^2 + 4q_1q_2 + 4q_2^2)/(q_1 + 2q_2)$, all of which are strictly positive (q_1 and q_2 are the force densities of cables and are therefore

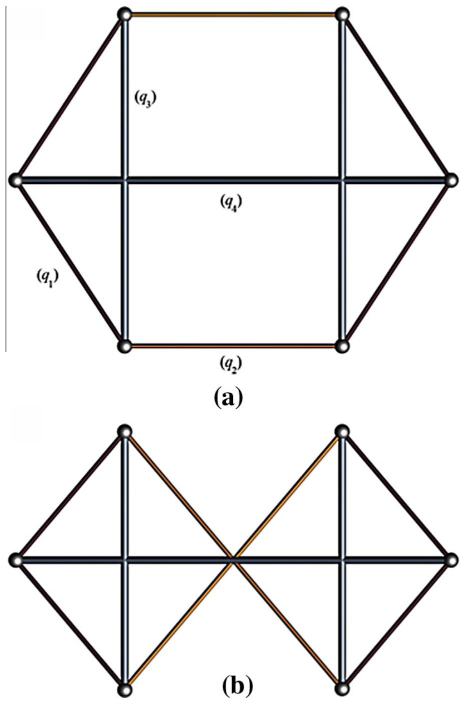

Fig. 4. Self-equilibrated configurations of a 2-dimensional tensegrity; (a) super-stable, (b) unstable.

positive). Hence, the force density matrix is semi-positive definite and the corresponding configuration is super-stable. For the second case, we also obtain three zero-valued eigenvalues. However, the first eigenvalue is $-2q_2$, which is clearly negative and leads to a configuration without super-stability. The other two eigenvalues are the same as those in the first case and are positive. As a result, our approach leads to results that are in complete agreement with those of the classic force density method.

At this stage, we select $q_1 = 2$, $q_2 = 1$ and $q_3 = q_4 = -1$ as the first typical case and $q_1 = 2$, $q_2 = 1$, $q_3 = -2$ and $q_4 = -1$ as the second typical case (both satisfying self-stress conditions) and calculate the nodal coordinates of tensegrity via Eq. (27). The configurations are shown in Fig. 4, where compressive elements are depicted in thick lines. Both configurations are symmetric without any dilation, shear or translation and all elements in each group have the same length.

6.2. Example 2

In this example, the analytical form-finding of a truncated tetrahedral tensegrity is studied. Fig. 5 shows a graph model of the tensegrity with node and element labelling. This graph has $n = 12$ nodes and $m = 24$ edges and its cyclomatic number is 13. The minimal cycle basis of this graph is formed using four 3-sided and nine 4-sided cycles, as summarised in Table 1. The proposed analytical process is applied to the combined form of the geometrical compatibility and equilibrium equations, leading to an upper triangular symbolic matrix ($\mathbf{H}'$).

It is possible to find three independent solutions for $\mathbf{d}_x$, $\mathbf{d}_y$ and $\mathbf{d}_z$ if the rank of $\mathbf{H}'$ is at most 21. Therefore, the 22nd–24th rows of $\mathbf{H}'$ should be zero. The simplified non-zero entries (numerators) found are

$$\mathbf{H}'(22,22) = 2\omega q_1\left(-2q_2^3 - 3q_1q_2^2 + 4q_2q_3^2 + 3q_1q_2q_3 + 3q_1q_3^2\right)$$

$$\mathbf{H}'(22,23) = \omega(9q_1^2q_2^2 + 3q_1^2q_2q_3 - 3q_1^2q_3 + 14q_1q_2^3 + 12q_1q_2^2q_3 \\ -4q_1q_2q_3^2 + 4q_2^4 + 8q_2^3q_3)$$

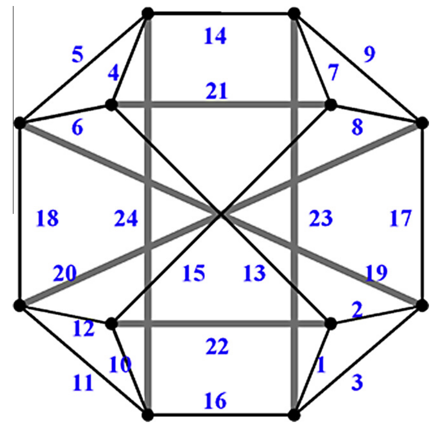

Fig. 5. Graph model of a truncated tetrahedral tensegrity.

$$\mathbf{H}'(22,24) = \omega\left(3q_1^2q_2^2 - 3q_1^2q_2q_3 + 3q_1^2q_3^2 + 6q_1q_2^3 + 4q_2^4\right)$$

$$\mathbf{H}'(23,23) = \omega(q_2)$$

$$\mathbf{H}'(23,24) = \omega(2q_3 - q_2)$$

$$\mathbf{H}'(24,24) = \omega$$

where $\omega = 3q_1^2q_2 + 3q_1^2q_3 + 2q_1q_2^2 + 6q_1q_2q_3 + 2q_1q_3^2 + 2q_2^2q_3 + 2q_2q_3^2$. All entries have a common sub-expression (ω), and $\omega = 0$ provides us with the rank deficiency required. The same equation has been provided in Zhang and Ohsaki (2012) for the self-stress state, verifying our results. The above equation can be simplified by setting $q_2 = \lambda q_1$ and $q_3 = \sigma q_1$, as follows:

$$\omega = 2(1+\lambda)\sigma^2 + (2\lambda(3+\lambda)+3)\sigma + \lambda(3+2\lambda) = 0$$

This gives another form of the self-stress condition for a truncated tetrahedral tensegrity, as described by Tibert and Pellegrino (2003). Note that, even though the force density matrix is symmetric and far smaller than our matrix, the analytical calculation of its eigenvalues (without exploiting symmetry) is impossible as a consequence of the Abel–Ruffini theorem (see Pesic, 2003) that there is no general algebraic solution to a polynomial equation of degree 5 or higher, while its factorisation using a Gauss elimination method leads to a matrix with highly complicated entries.

Using the equations provided, we consider two sets of typical force densities, $q_1 = q_2 = 1$, $q_3 = (-11 \pm \sqrt{41})/8$, and calculate the corresponding nodal coordinates. In the self-stressed state, all nodes of tensegrities are located on spheres (whose centres are the origin of the coordinate system) with radii of 0.2970 and 0.1998 for cases (a) and (b), respectively. Fig. 6 illustrates the two configurations mentioned above, where the first case is super-stable.

6.3. Example 3

This example has been selected from Tran and Lee (2010a). The original problem is the form-finding of a cable-strut structure with some fixed nodes. Dummy members have been added to the structure to convert it to an equivalent model without fixed nodes (external continuous compressive elements in Fig. 7). We adopt the same labelling of elements, nodes and element groupings as in the above reference.

Note that all elements are grouped into four sets, including two groups of tensile elements (10 elements in each group) and two groups of compressive elements (5 elements in each group). In

Table 1
Set of the minimal cycle basis for a truncated tetrahedral tensegrity.

Cycle name	c_1	c_2	c_3	c_4	c_5	c_6	c_7	c_8	c_9	c_{10}	c_{11}	c_{12}	c_{13}
Element number	1^+	4^+	7^+	10^+	3^+	5^+	1^+	4^+	13^+	19^+	23^+	2^+	15^+
	2^+	5^+	8^+	11^+	17^+	18^+	22^+	14^+	21^+	18^+	14^-	19^+	12^+
	3^-	6^-	9^-	12^-	9^-	11^-	10^+	7^+	15^+	20^-	24^+	6^-	20^-
					23^-	24^-	16^-	21^-	22^-	17^-	16^-	13^-	8^-

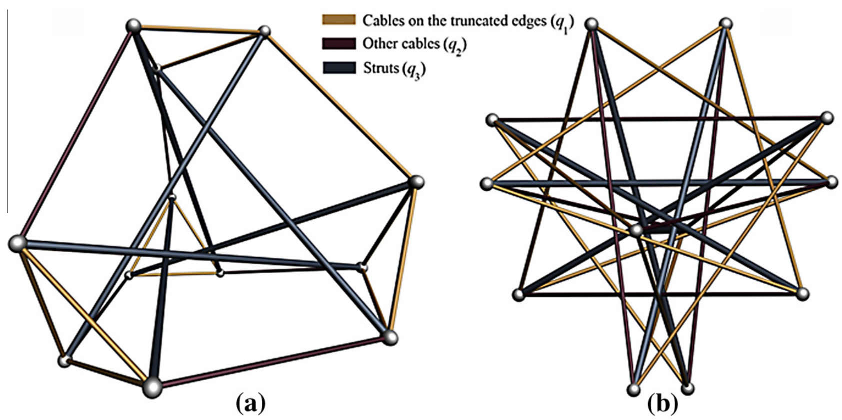

Fig. 6. Self-equilibrated configurations of a truncated tetrahedral tensegrity (a) $q_3 = (-11 + \sqrt{41})/8$; (b) $q_3 = (-11 - \sqrt{41})/8$.

addition, q_1 and q_2 are considered the force densities of elements in the tensile groups (the first and second groups), while q_3 and q_4 are considered the force densities of elements in the compressive groups (the third and fourth groups). Force densities of typical elements are shown in Fig. 7, where different colours illustrate elements of different groups.

Our numerical form-finding method successfully generates two different forms. Both configurations are illustrated in Fig. 7. For this example, the numerical procedure proposed by Tran and Lee (2010a) gave a self-stressed configuration without super-stability. Table 2 provides more details about our form-finding procedure, where force densities are ordered from q_1 to q_4 . Both cases converged in just two iterations, demonstrating the efficiency of our proposed method (this rate is constant for every initial set of force densities).

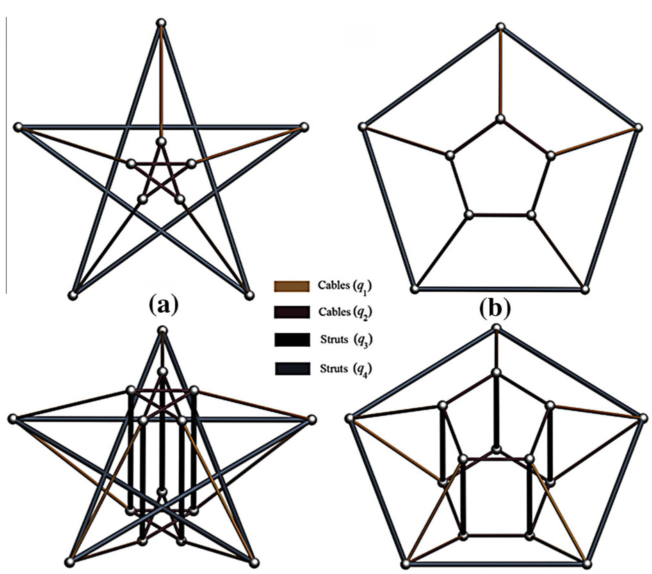

Fig. 7. Top and perspective views of two self-equilibrated configurations for Example 3 (a) super-stable (b) not super-stable.

We also analytically investigate the conditions for a valid form in this example using our formulation. The rank deficiency of the combined form of the equilibrium and geometrical compatibility conditions provides two different equations: $q_1 + 2q_3 = 0$ and $4q_1^2q_2^2 + 4q_1^2q_2q_4 + q_1^2q_4^2 + 10q_1q_2^2q_4 + 5q_1q_2q_4^2 + 5q_2^2q_4^2 = 0$. The second equation can be rewritten in a simpler form using new variables: $q_2 = \alpha q_1$ (α is positive) and $q_4 = \beta q_1$ (β is negative). The equation is then rewritten as follows:

$$(4 + 10\beta + 5\beta^2)\alpha^2 + (4\beta + 5\beta^2)\alpha + \beta^2 = 0$$

This equation has two roots:

$$\alpha = -\frac{4\beta + (5 \pm \sqrt{5})\beta^2}{8 + 20\beta + 10\beta^2}$$

Only positive roots are acceptable. Our numerical results are in complete agreement with the established analytical equations, verifying the accuracy of the results.

6.4. Example 4

In this example, the numerical form-finding of a well-known tensegrity, based on a truncated icosahedron, is studied using the proposed method. This tensegrity has $n = 60$ nodes and $m = 120$ elements. The reader may refer to Murakami and Nishimura (2001) for more detail on the connectivity and symmetry properties of this tensegrity. The cyclomatic number for a graph of this tensegrity is 61, meaning that 61 geometrical compatibility equations (or independent cycles) should be generated for this model. For this example, we numerically generate the coefficient matrix of the geometrical compatibility equations ($\mathbf{C}$) by calculating a triangular null-space basis of the node-member incidence matrix. Three cases are studied using our numerical method; the first case converges to a super-stable configuration, while the others only satisfy the self-equilibrium condition. The detailed results of the numerical procedure are summarised in Table 3.

Table 2
Detailed results of the numerical form-finding method for Example 3.

	Initial random force densities	Final normalised force densities	Total number of iterations and t
Case 1 (super stable)	0.6110	0.2091	**2**, 3.3074×10^{-16}
	0.7788	0.2160	
	−0.4235	−0.1045	
	−0.0908	−0.0912	
Case 2	0.6619	0.1793	**2**, 3.4619×10^{-16}
	0.7703	0.2243	
	−0.3502	−0.0896	
	−0.6620	−0.1644	

Table 3
Detailed results of the numerical form-finding method for Example 4.

	Initial random force densities	Final normalised force densities	Total number of iterations and t
Case 1 (super stable)	0.8055	0.1137	**67**, 6.2985×10^{-16}
	0.5767	0.0780	
	−0.1829	−0.0375	
Case 2	0.7127	0.1077	**9**, 9.4048×10^{-16}
	0.5005	0.0826	
	−0.4711	−0.0575	
Case 3	0.0714	0.0245	**7**, 5.3331×10^{-16}
	0.5216	0.1766	
	−0.0967	−0.0307	

We confirm all our results with the analytical self-stress conditions recently derived by Zhang et al. (2012) for truncated icosahedral tensegrities, as follows:

$$q_s^2 q_b + q_s q_b^2 + \frac{5-\sqrt{5}}{5}(q_s^2 + q_b^2) + \frac{3(5-\sqrt{5})}{5} q_s q_b + \frac{3-\sqrt{5}}{2}(q_s + q_b) = 0$$

$$q_s^2 q_b + q_s q_b^2 + \frac{5+\sqrt{5}}{5}(q_s^2 + q_b^2) + \frac{3(5+\sqrt{5})}{5} q_s q_b + \frac{3+\sqrt{5}}{2}(q_s + q_b) = 0$$

Note that q_s and q_b are force densities of cables and struts that have been normalised based on the force density of cables on truncated edges, i.e. $q_s = q_2/q_1$ and $q_b = q_3/q_1$. The force densities obtained for the first case (super-stable) are in complete agreement with the first equation above (see also Koohestani, 2012; Murakami and Nishimura, 2001; Zhang et al., 2013), while the other two cases exactly satisfy the second equation. This verifies the accuracy of our method.

Fig. 8 illustrates the final geometries of the tensegrity in the three cases examined. All nodes of the tensegrity are located on

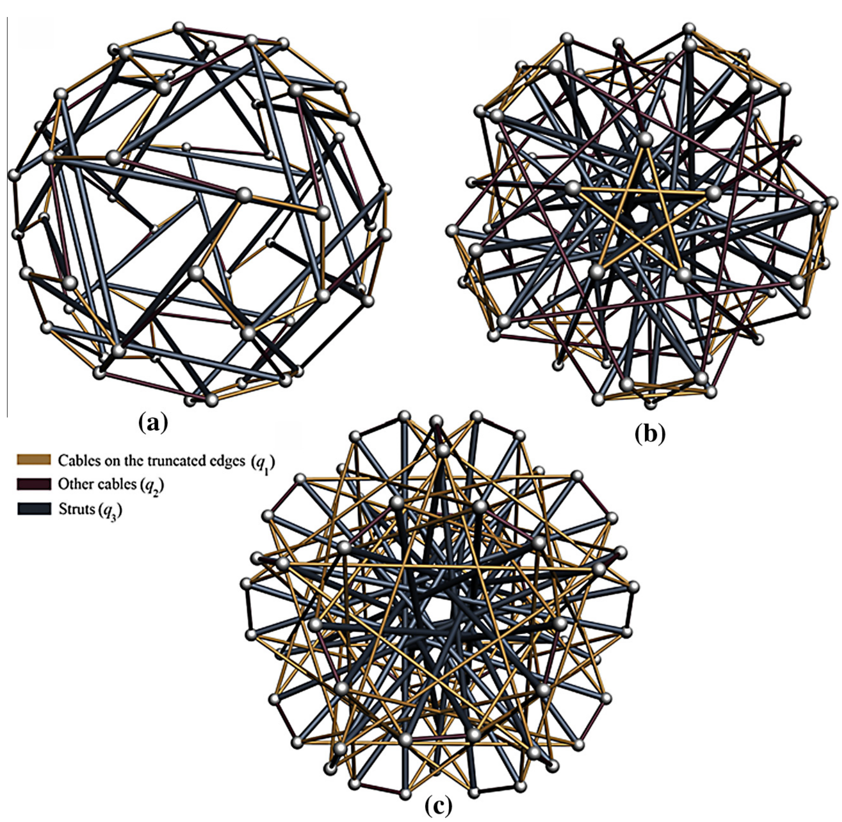

Fig. 8. Self-equilibrated configurations of a truncated icosahedral tensegrity (a) case 1, super-stable; (b) case 2, not super-stable; (c) case 3, not super-stable.

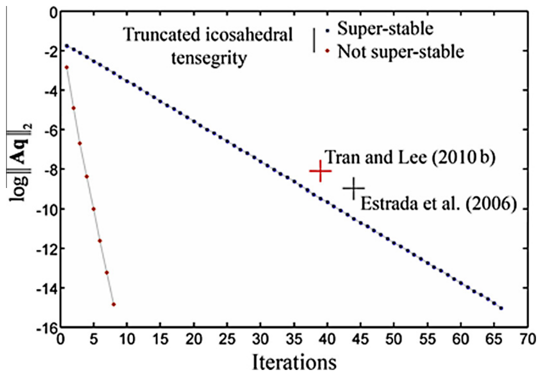

Fig. 9. Comparison of the convergence history of the our numerical method with those of the other methods for truncated icosahedral tensegrity.

spheres with centres at the origin of the coordinate system and radii of 0.2190, 0.1286 and 0.1107 for cases 1, 2 and 3, respectively. Our method directly generates geometries without any dilation, shear or translation, and where all elements in each group have the same length. Furthermore, the performance of the present method in terms of convergence is studied in this example. To do so, we perform 20 runs of our numerical form-finding method for both cases (with and without super-stability) with different random sets of force densities.

Fig. 9 illustrates a comparison of the convergence history of the proposed method (average of 20 runs) and those of Tran and Lee (2010b) and Estrada et al. (2006). The comparison clearly verifies the efficiency of the proposed method.

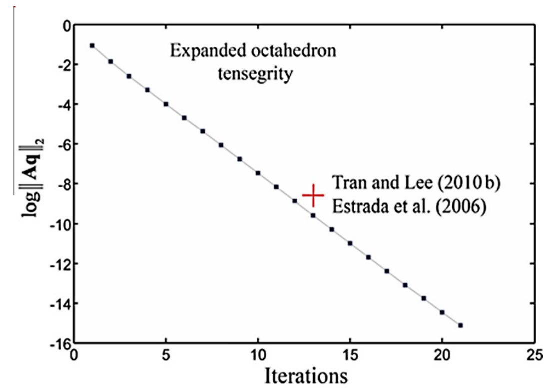

Fig. 11. Comparison of the convergence history of the our numerical method with those of the other methods for the "expanded octahedron" tensegrity.

6.5. Example 5

The numerical form-finding of the "expanded octahedron" tensegrity is studied in this example. This tensegrity has $n = 12$ nodes and $m = 30$ elements. The coefficient matrix of the geometrical compatibility equations is calculated numerically. We choose only two variables by considering the force density of all the cables (q_1) as one variable and that of all the struts (q_2) as the other. For this initialisation, our method generates a super-stable configuration (see Fig. 10(a)) with a constant q_1/q_2 ratio of $-2/3$. The results given for this structure are in a complete agreement with those of Tibert and Pellegrino (2003). The convergence history of our numerical method is provided in Fig. 11.

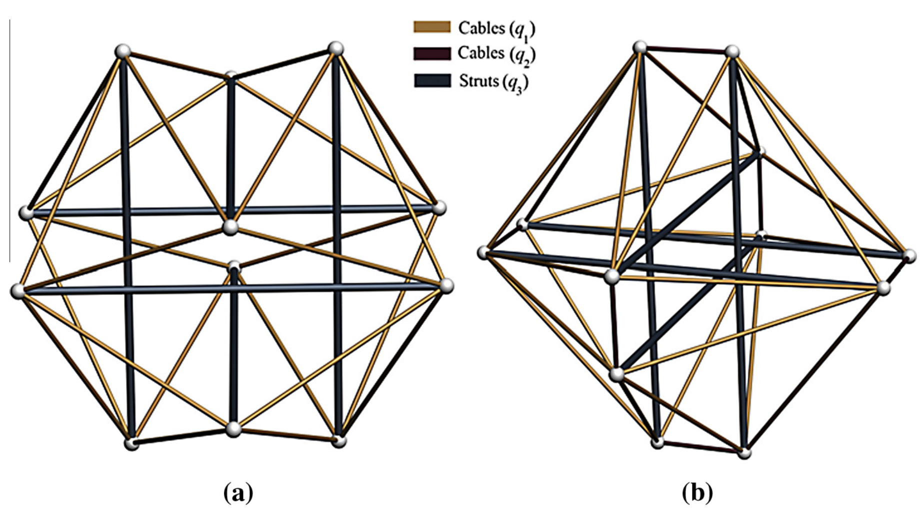

Fig. 10. A super-stable (a) expanded and (b) modified "expanded octahedron" tensegrities.

Table 4
Detailed results of the numerical form-finding method for Example 5.

	Initial random force densities	Final normalised force densities	Total number of iterations and t
Case 1 (super stable)	0.2208	0.1129	**2**, 4.0361×10^{-16}
	0.4536	0.2748	
	−0.4653	−0.2004	
Case 2 (super stable)	0.4061	0.1030	**2**, 3.7118×10^{-16}
	0.6580	0.1723	
	0.5752	0.1404	
	0.9760	0.1777	
	−0.4416	−0.2147	
	−0.7778	−0.2659	
	−0.5695	−0.2200	

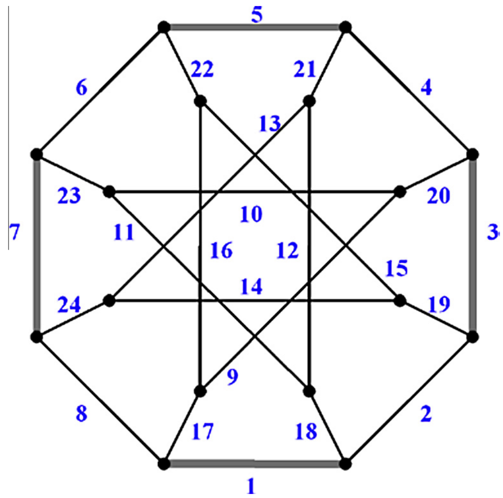

Fig. 12. Möbius–Kantor graph with labelling.

We slightly change this example in order to demonstrate the capability of our built-in grouping and numerical approach to deal with tensegrities having multiple states of self-stress. To do so, 6 members (connecting end of parallel compressive elements) have been added to the original model of the "expanded octahedron". This tensegrity has been studied by Tran and Lee (2011) for a case of multiple states of self-stress (the structure has six states of self stress). We study this example through our numerical approach and also note that, we adopt the same labelling of nodes and elements as the above reference. Two cases have been considered based on two different groupings of elements. In the first case, all elements are grouped into three sets, including two groups of cables $g_1 = \{1, 2, \ldots, 24\}$ and $g_2 = \{25, 26, \ldots, 30\}$ and, a group of struts $g_3 = \{31, 32, \ldots, 36\}$ as in Tran and Lee (2011).

Furthermore, in order to show the viability of our method, we consider a more complex grouping of elements. In this case, all elements are packed into seven groups with the corresponding force densities $q_1 - q_7$. These groups are $g_1 = \{1, 2, 7, 8, 13, 15, 18, 20\}$, $g_2 = \{3, 4, 5, 6, 21, 22, 23, 24\}$, $g_3 = \{9, 10, 11, 12, 14, 16, 17, 19\}$ and $g_4 = \{25, 26, 27, 28, 29, 30\}$ for cables and $g_5 = \{31, 32\}$, $g_6 = \{33, 36\}$ and $g_7 = \{34, 35\}$ for struts. Our numerical form-finding method with its built-in grouping scheme directly generates feasible sets of force densities for both cases (both are super-stable) in just 2 iterations. This can be compared with the 18 iterations required by the two-stage algorithm of Tran and Lee (2011) for the first case. Table 4 provides more details about the form-finding process. The equilibrium configuration of the first case is also illustrated in Fig. 10(b).

6.6. Example 6

All the examples presented so far are known tensegrities that have been studied in the literature. In this example we try to demonstrate the capacity of the proposed methods for form-finding and exploring new tensegrities. Fig. 12 shows a well-known graph (called the generalised Peterson graph $G(8,3)$ or Möbius–Kantor graph (Coxeter, 1950), with $n = 16$ nodes, $m = 24$ edges and $\beta = 9$ independent cycles. We select this graph as the topology of a tensegrity and consider two cases based on different groupings of edges. In the first case, we consider five groups of elements, one set of struts $g_1 = \{1, 3, 5, 7\}$ and four sets of cables $g_2 = \{2, 4, 6, 8\}$, $g_3 = \{9, 11, 13, 15\}$, $g_4 = \{10, 12, 14, 16\}$ and $g_5 = \{17, 18, \ldots, 24\}$. In the second case, three groups of elements, one set of struts $g_1 = \{1, 3, 5, 7\}$ and two sets of cables $g_2 = \{2, 4, 6, 8, 9, 11, 13, 15\}$ and $g_3 = \{10, 12, 14, 16, 17, \ldots, 24\}$ are considered. Furthermore, q_i is associated with g_i as its respective force density. Note that, this type of grouping leaves eight nodes of the tensegrity without any compressive element which

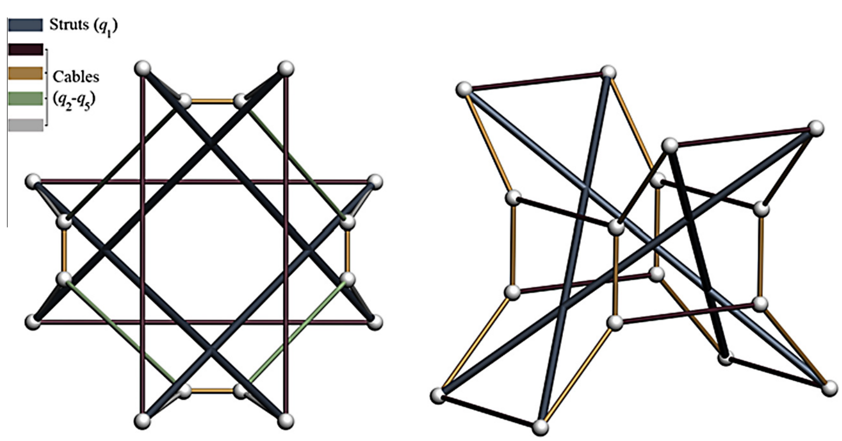

Fig. 13. Two new super-stable tensegrities (a) case 1, (b) case 2.

Table 5
Detailed results of the numerical form-finding method for Example 6.

	Initial random force densities	Final normalised force densities	Total number of iterations and t
Case 1 (super stable)	−0.0900	−0.0449	**65**, 7.7232×10^{-16}
	0.1117	0.0089	
	0.6787	0.3300	
	0.1363	0.0686	
	0.4952	0.2591	
Case 2 (super stable)	−0.2967	−0.0877	**151**, 8.5503×10^{-16}
	0.3188	0.1316	
	0.4242	0.2631	

makes it rather different from classical tensegrities. We found two super-stable configurations for both cases, as shown in Fig. 13.

Table 5 also provides the detailed results of the form-finding for both cases, each for two random sets of force densities. Furthermore, by examining the numerical results, we found that in the second case, three force densities are related to each other through very simple relationships $q_1 = -q_3/3$ and $q_2 = q_3/2$. These relationships have also been verified through the analytical approach presented.

7. Discussions and conclusions

In this section, we discuss the advantages and disadvantages of our method in comparison with other available methods and formulations. We have introduced a combined formulation of the equilibrium and geometrical compatibility equations, which offers a new insight into the form-finding of tensegrity structures. The proposed formulation is, in fact, the natural counterpart of the force density method, but with different structure and variables. Our analytical results are in complete agreement with those of Tibert and Pellegrino (2003), Zhang et al. (2012) and Zhang and Ohsaki (2012). Clearly, the new structure of the combined formulation enables us to find reasonable analytical solutions for moderately large and irregular models. This advantage, for instance, is shown in examples 6.2 and 6.3 where fairly simple analytical relationships have been obtained for the tensegrities. For these examples, analytical computation using the force density matrix is far more difficult. Our numerical approach iteratively employs the SVD of two different forms of equilibrium equations to find a state of self-stress. This part of our numerical method is related to the methods developed by Estrada et al. (2006) and Tran and Lee (2010a,b), but it is different from the adaptive force density method of Zhang and Ohsaki (2006). In general, the numerical approach presented in this paper has several distinct advantages in comparison with those studies mentioned above including:

(a) It starts from a random set of force densities (instead of using a constant prototype vector containing only +1 and −1). This enables us to form and explore a wide variety of tensegrities with or without super-stability and with different levels of energies. This feature may also be very important for the design and optimisation of tensegrities with different constraints.
(b) Our experiments show that the method presented is accurate, and it has good convergence performance (i.e. it converges faster than similar methods such as Estrada et al., 2006; Tran and Lee, 2010b, 2011)
(c) The combined form of the equilibrium and compatibility equations with Cartesian components of element lengths as primary variables enable us to directly form a symmetric geometry for a symmetric tensegrity. All the numerical methods mentioned above usually require secondary computations to form a symmetric tensegrity even from a symmetric set of force densities.
(d) The method is enriched with a special grouping scheme, which allows us to directly apply the symmetry properties of tensegrities to the form-finding process. Therefore, as demonstrated in example 5, our method can effectively and efficiently generate a single (integral) feasible set of force densities for different groupings.

Our method has two weak points. First, the method does not have a built-in strategy to guide the solution towards super-stable (or at least stable) configurations (or tensegrities with different levels of energy). In other words, by starting from a random set of force densities, the method converges to a super-stable or not super-stable form randomly. Second, the method may converge to a solution which is not feasible (the force density or the length of some of elements is zero). The conditions which lead to such a situation have been discussed in Section 5.4. However, we believe that this weakness is not significant, and it can be easily resolved by setting a new starting point (new set of random force densities).

In general, this study reveals that our formulation and its associated analytical and numerical methods provide an appealing platform for the study of tensegrity structures. However, investigating the super-stability conditions via the combined formulation, evaluating the performance of the numerical method for the form-finding of irregular tensegrities and the form-finding and optimisation of tensegrities under different constraints may be important enough to call for new studies.

References

Berge, C., 2001. The Theory of Graphs. Dover, New York.
Chen, Y., Feng, J., Wu, Y., 2012. Novel form-finding of tensegrity structures using ant colony systems. ASME J. Mech. Robot. 4 (3). Article No. 031001.
Connelly, R., 1982. Rigidity and energy. Invent. Math. 66, 11–33.
Connelly, R., Terrell, M., 1995. Globally rigid symmetric tensegrities. Struct. Topol. 21, 59–78.
Coxeter, H.S.M., 1950. Self-dual configurations and regular graphs. Bull. Am. Math. Soc. 56, 413–455.
De Pina, J.C., 1995. Applications of Shortest Path Methods. PhD thesis, University of Amsterdam, Netherlands.
Ehara, S., Kanno, Y., 2010. Topology design of tensegrity structures via mixed integer programming. Int. J. Solids Struct. 47, 571–579.
Estrada, G.G., Bungartz, H.J., Mohrdieck, C., 2006. Numerical form-finding of tensegrity structures. Int. J. Solids Struct. 43, 6855–6868.
Fuller, R.B., 1962. Tensile-integrity structures, United States Patent 3,063,521, November 13.
Golub, G.H., Van Loan, C.F., 1996. Matrix Computations, third ed. Johns Hopkins University Press, Baltimore.
Guest, S., 2006. The stiffness of prestressed frameworks: a unifying approach. Int. J. Solids Struct. 43, 842–854.
Hernàndez Juan, J., Mirats Tur, J.M., 2008. Tensegrity frameworks: static analysis review. Mech. Mach. Theory 43, 859–881.
Horton, J.D., 1987. A polynomial-time algorithm to find the shortest cycle basis of a graph. SIAM J. Comput. 16, 358–366.
Kanno, Y., 2011. Topology optimisation of tensegrity structures under compliance constraint: a mixed integer linear programming approach. Optim. Eng.. http://dx.doi.org/10.1007/s11081-011-9172-0, in press.
Kanno, Y., 2012. Toplogy optimisation of tensegrity structures under self-weight loads. J. Oper. Res. Soc. Jpn. 55, 125–145.
Kaveh, A., 2004. Structural Mechanics: Graph and Matrix Methods, third ed. Research Studies Press, Wiley, UK.
Kavitha, T., Mehlhorn, K., Michail, D., Paluch, K.E., 2008. An $\tilde{O}(m^2 n)$ algorithm for minimum cycle basis of graphs. Algorithmica 52, 333–349.
Koohestani, K., 2012. Form-finding of tensegrity structures via genetic algorithm. Int. J. Solids Struct. 49, 739–747.
Li, Y., Feng, X.Q., Cao, Y.P., Gao, H., 2010. A Monte Carlo form-finding method for large scale regular and irregular tensegrity structures. Int. J. Solids Struct. 47, 1888–1898.
Masic, M., Skelton, R.E., Gill, P.E., 2005. Algebraic tensegrity form-finding. Int. J. Solids Struct. 42, 4833–4858.
Mehlhorn, K., Michail, D., 2009. Minimum cycle bases: faster and simpler. ACM Trans. Algorithm 6 (1), 1–13.
Micheletti, A., 2008. On generalised reciprocal diagrams for self-stressed frameworks. Int. J. Space Struct. 23, 153–166.
Mirats Tur, J.M., Hernàndez Juan, S., 2009. Tensegrity frameworks: dynamic analysis review and open problems. Mech. Mach. Theory 44, 1–18.
Motro, R., 1984. Forms and forces in tensegrity systems. In: Nooshin, H. (Ed.), Proceedings of Third International Conference on Space Structures. Elsevier, Amsterdam, pp. 180–185.
Murakami, H., Nishimura, Y., 2001. Static and dynamic characterization of regular truncated icosahedral and dodecahedral tensegrity modules. Int. J. Solids Struct. 38, 9359–9381.
Ohsaki, M., Zhang, J.Y., 2006. Stability conditions of prestressed pin-jointed structures. Int. J. Nonlinear Mech. 41, 1109–1117.
Pagitz, M., Mirats Tur, J.M., 2009. Finite element based form-finding algorithm for tensegrity structures. Int. J. Solids Struct. 46, 3235–3240.
Patnaik, S.N., 1986. The integrated force method vs the standard force method. Comput. Struct. 22, 151–163.
Paul, C., Lipson, H., Cuevas, F.J.V., 2005. Evolutionary form-finding of tensegrity structures. In: Proceedings of the 2005 Conference on Genetic and Evolutionary Computation, ACM, Washington, USA.
Pellegrino, S., 1986. Mechanics of kinematically indeterminate structures, Ph.D. Dissertation, University of Cambridge, UK.

Pellegrino, S., 1993. Structural computations with the singular-value decomposition of the equilibrium matrix. Int. J. Solids Struct. 30, 3025–3035.

Pellegrino, S., Calladine, C.R., 1986. Matrix analysis of statically and kinematically indeterminate frameworks. Int. J. Solids Struct. 22, 409–428.

Pesic, P., 2003. Abel's Proof: An Essay on the Sources and Meaning of Mathematical Unsolvability. MIT Press, Cambridge, MA.

Rieffel, J., Cuevas, F.V., Lipson, H., 2009. Automated discovery and optimization of large irregular tensegrity structures. Comput. Struct. 87, 368–379.

Schek, H.J., 1974. The force density method for form finding and computation of general networks. Comput. Methods Appl. Mech. Eng. 3, 115–134.

Snelson, K.D., 1965. Continuous tension, discontinuous compression structures, United States Patent 3,169,611, February16.

Soyer, E., Topçu, A., 2001. Sparse self-stress matrices for finite element force method. Int. J. Numer. Methods Eng. 50, 2175–2194.

Sultan, C., 1999. Modelling, design and control of tensegrity structures with applications, Ph.D. Dissertation, Purdue University.

Sultan, C., 2009. Tensegrity: 60 years of art, science, and engineering. In: Aref, H., van der Giessen, E. (Eds.), Advances in Applied Mechanics, 43. Elsevier Academic Press Inc, San Diego, CA, pp. 69–145.

Sultan, C., Corless, M., Skelton, R.E., 1999. Reduced prestressability conditions for tensegrity structures. In: Proceedings of 40th AIAA/ASME/ASCE/AHS/ASC Structures, Structural Dynamics and Materials Conference, 12–15 April 1999, St Louis, MO, AIAA.

Sultan, C., Corless, M., Skelton, R.E., 2001. The prestressability problem of tensegrity structures: some analytical solutions. Int. J. Solids Struct. 38, 5223–5255.

Tibert, A.G., Pellegrino, S., 2003. Review of form finding methods for tensegrity structures. Int. J. Space Struct. 18 (4), 209–223.

Tran, H.C., Lee, J., 2010a. Advanced form-finding for cable-strut structures. Int. J. Solids Struct. 47, 1785–1794.

Tran, H.C., Lee, J., 2010b. Advanced form-finding of tensegrity structures. Comput. Struct. 88, 237–246.

Tran, H.C., Lee, J., 2011. Form-finding of tensegrity structures with multiple states of self-stress. Acta Mech. 222, 131–147.

Xu, X., Luo, Y., 2010. Form-finding of nonregular tensegrities using genetic algorithm. Mech. Res. Commun. 37, 85–91.

Zhang, J.Y., Ohsaki, M., 2006. Adaptive force density method for form-finding problem of tensegrity structures. Int. J. Solids Struct. 43, 5658–5673.

Zhang, J.Y., Ohsaki, M., 2007. Stability conditions for tensegrity structures. Int. J. Solids Struct. 44, 3875–3886.

Zhang, J.Y., Ohsaki, M., 2012. Self-equilibrium and stability of regular truncated tetrahedral tensegrity structures. J. Mech. Phys. Solids 60, 1757–1770.

Zhang, J.Y., Ohsaki, M., Kanno, Y., 2006. A direct approach to design of geometry and forces of tensegrity systems. Int. J. Solids Struct. 43, 2260–2278.

Zhang, J.Y., Guest, S.D., Ohsaki, M., 2009a. Symmetric prismatic tensegrity structures: Part I. Configuration and stability. Int. J. Solids Struct. 46, 1–14.

Zhang, J.Y., Guest, S.D., Ohsaki, M., 2009b. Symmetric prismatic tensegrity structures: Part II. Symmetry-adapted formulations. Int. J. Solids Struct. 46, 15–30.

Zhang, J.Y., Guest, S.D., Connelly, R., Ohsaki, M., 2010. Dihedral 'star' tensegrity structures. Int. J. Solids Struct. 47, 1–9.

Zhang, L.Y., Li, Y., Cao, Y.P., Feng, X.Q., Gao, H., 2012. Self-equilibrium and super-stability of truncated regular polyhedral tensegrity structures: a unified analytical solution. Proc. R. Soc. A 468, 3323–3347.

Zhang, L.Y., Li, Y., Cao, Y.P., Feng, X.Q., 2013. A unified solution for self-equilibrium and super-stability of rhombic truncated regular polyhedral tensegrities. Int. J. Solids Struct. 50, 234–245.